

Origin of the large voltage-controlled magnetic anisotropy in a Cr/Fe/MgO junction with an ultrathin Fe layer: First-principles investigation

W. Z. Chen,^{1,2} L. N. Jiang,¹ Z. R. Yan,¹ Y. Zhu,^{1,3} C. H. Wan,¹ and X. F. Han^{1,2,4,*}

¹Beijing National Laboratory for Condensed Matter Physics, Institute of Physics, University of Chinese Academy of Sciences, Chinese Academy of Sciences, Beijing 100190, China

²Center of Materials Science and Optoelectronics Engineering, University of Chinese Academy of Sciences, Beijing 100049, China

³Key Laboratory of Physics and Technology for Advanced Batteries (Ministry of Education), Department of Physics, Jilin University, Changchun 130012, People's Republic of China

⁴Songshan Lake Materials Laboratory, Dongguan, Guangdong 523808, China



(Received 16 December 2019; revised manuscript received 4 March 2020; accepted 31 March 2020; published 27 April 2020)

Voltage-controlled magnetic anisotropy (VCMA) has attracted broad interest due to its high efficiency in switching magnetization. Large VCMA was experimentally observed in Cr/Fe/MgO junction with ultrathin Fe layer [Nozaki *et al.*, *Phys. Rev. Appl.* **5**, 044006 (2016)], whose underlying mechanism was still not clear however. The Cr/Fe/MgO/Fe magnetic tunnel junction (MTJ) is also well known for its quantum-well (QW) states and as-induced spin-dependent resonant tunneling [Greullet *et al.*, *Phys. Rev. Lett.* **99**, 187202 (2007)]. Here, in order to uncover the relation between the large VCMA and the QW states, we developed a k -resolved VCMA calculation method combined with the second-order perturbation theory to investigate it. We find the VCMA coefficient reaches -297 fJ/V m matching well with the previous experiment with three monolayers (MLs) of Fe. The coefficient oscillates strongly and even changes its sign with increasing the number of Fe MLs. Comparing the k -resolved VCMA with the Fermi surface of the interfacial Fe atom, the screening charges theory for VCMA was verified. For 2–9 MLs Fe, interestingly, the QW states of Δ_1 electron at the Γ point provide large (no) contribution to the VCMA with odd (even) MLs. Moreover, the change of the orbital-resolved Fermi surface at the interfacial Fe atom also plays an important role on VCMA oscillation, which as well as the QW states results in the largest VCMA for 3-ML Fe. Our results deepen the understanding of the large VCMA in the Cr/Fe/MgO junction, which would be helpful to design a practical MTJ with large VCMA.

DOI: [10.1103/PhysRevB.101.144434](https://doi.org/10.1103/PhysRevB.101.144434)

I. INTRODUCTION

Voltage-controlled magnetic anisotropy (VCMA) enables one to apply electric field rather than current to efficiently switch or manipulate magnetization without Joule heating [1–9]. In magnetic random access memories (MRAMs), VCMA can assist spin-transfer torque or spin-orbit torque switching [10,11] or directly be applied in precessional switching by well-defined voltage pulse [12,13]. For both applications, large VCMA is desired.

There are several strategies to achieve large VCMA. Voltage-driven ionic reactions can contribute giant VCMA of 5 pJ/Vm [14,15] but with slow speed. Ferroelectricity or piezoelectricity provides another solution [13,16] but with limited endurance. Electric field across a magnetic tunnel junction (MTJ) can redistribute electrons near the interface, which directly serves as a third manner to produce large VCMA. Besides, Fe/MgO/Fe or CoFeB/MgO/CoFeB MTJ has been widely used in MRAM owing to its high tunnel magnetoresistance ratio [17–20] and perpendicular magnetic anisotropy [21,22]. Thus it seems appealing to realize large

VCMA directly in Fe/MgO/Fe MTJs, which shares compatibility with current MRAM technology [23–27].

Recently, large VCMA up to 290 fJ/Vm in Cr/Fe/MgO with ultrathin Fe layer (0.44 nm or 3 MLs) was obtained in experiment [28–30], while it was 23 fJ/V m in V/Fe(0.5 nm)/MgO [24] and around 30 fJ/V m in Ta/CoFeB(1 nm)/MgO junctions [31]. This VCMA seemingly relies on the species of the underlayer. Furthermore, it depends sensitively on Fe thickness (t_{Fe}) and sharply degrades to less than 100 fJ/V m for 0.69 nm Fe. Cr/Fe/MgO/Fe MTJ has also been studied extensively in the past decades because of quantum-well (QW) states and as-induced spin-dependent resonant tunneling in it [32–36]. Here the QW states are composed by the Δ_1 states at Γ point of Brillouin zone from the thin Fe layer between Cr and MgO because there exists a gap for Cr Δ_1 states. The number of the QW states depends on the number of Fe monolayers (MLs); the thinner Fe layer leads to the sparser QW states. Then the following question whether the large VCMA correlates with the QW states naturally emerges.

In order to answer the question, we developed a first-principles k -resolved VCMA calculation method, combining the second-order perturbation theory and partial density of states (PDOS) analysis at Γ point. This method enabled us to

*Corresponding author: xfhan@iphy.ac.cn

clearly uncover the origin of the large VCMA in Cr/Fe/MgO junctions. Calculated VCMA reached -297 fJ/V m for 3-ML Fe, matching experiment well [28]. Furthermore it oscillated from negative to positive with the increase in t_{Fe} . The screening charge theory for VCMA [4,27] was verified through comparison between k -resolved VCMA and the Fermi surface of interfacial atoms. More importantly, the QW states as well as electron redistribution near the Fermi energy resulted in the VCMA oscillation and the largest VCMA for 3-ML Fe. The interfacial resonance states (IRSs) at the Fe/MgO interface [17] also contributed some hot spots for the k -resolved VCMA. Our results might guide a design of optimized MTJs with giant VCMA performance.

II. METHOD

The magnetocrystalline anisotropy (MCA) energy is calculated by the force theorem approach [37]. Within this theorem, a non-self-consistent calculation including spin-orbit coupling (SOC) is performed for a given orientation of magnetic moment with a fixed charge density obtained from a self-consistent calculation in the absence of SOC. With the Methfessel-Paxton smearing method for electron states occupation, the MCA energy is composed by two terms:

$$MCA = F^\parallel - F^\perp = \Delta E_e - T \Delta S, \quad (1)$$

where F^\perp (F^\parallel) represents the free energy for out-of-plane (in-plane) magnetization orientation with respect to the interface, and ΔE_e (ΔS) is the difference of band energy (entropy) from out-of-plane to in-plane magnetization orientation. ΔE_e can be resolved in the two-dimensional Brillouin zone,

$$\begin{aligned} \Delta E_e(k) &= \sum_n \varepsilon_{nk}^\parallel f_{nk}^\parallel - \varepsilon_{nk}^\perp f_{nk}^\perp = \Delta E_\varepsilon(k) + \Delta E_f(k), \\ E_\varepsilon(k) &= \sum_n (\varepsilon_{nk}^\parallel - \varepsilon_{nk}^\perp) \frac{(f_{nk}^\parallel + f_{nk}^\perp)}{2}, \\ E_f(k) &= \sum_n \frac{(\varepsilon_{nk}^\parallel + \varepsilon_{nk}^\perp)}{2} (f_{nk}^\parallel - f_{nk}^\perp), \end{aligned} \quad (2)$$

where ε_{nk} (f_{nk}) is the eigenvalue (occupation number) for the n th band with wave vector k . We divide it into two parts as shown in the above formula. ΔE_ε means the energy originated from the change of eigenvalue on the order of meV. ΔE_f means the energy that results from the electron transfer among k points and it is on the order of eV. We will prove that the k -resolved MCA energy can be exactly equal to ΔE_ε in the following. Because the variation of free energy F with respect to occupation number f_{nk} should be zero, we get

$$\frac{\partial F}{\partial f_{nk}} = \frac{\partial E_e}{\partial f_{nk}} - \frac{T \partial S}{\partial f_{nk}} = 0. \quad (3)$$

Integrating over all k and n ,

$$\sum \frac{\partial F}{\partial f_{nk}} \Delta f_{nk} = \sum \varepsilon_{nk} \Delta f_{nk} - T \Delta S = 0. \quad (4)$$

This means that $\Delta E_f \approx T \Delta S$ as Δf_{nk} is small enough. Therefore, there is the k -resolved MCA energy,

$$MCA(k) \approx \Delta E_e(k) = \sum_n (\varepsilon_{nk}^\parallel - \varepsilon_{nk}^\perp) \frac{(f_{nk}^\parallel + f_{nk}^\perp)}{2}. \quad (5)$$

Next, we deduce the second-order perturbation theory of SOC for MCA at a specific wave vector k . Within the Bloch representation, the Hamiltonian including SOC for a single k point is given by

$$\begin{aligned} H_k &= -\frac{\hbar^2}{2m} \nabla^2 + \frac{\hbar^2}{2m} k \cdot \hat{p} + \frac{\hbar^2 k^2}{2m} + V(r) \\ &+ \hbar \xi \hat{\sigma} \cdot (\hat{r} \times k) + \xi \hat{\sigma} \cdot \hat{L}, \end{aligned} \quad (6)$$

where \hbar is the reduced Planck constant, m is the electron mass, $V(r)$ is the crystal potential, and ξ is the SOC constant. The fifth and sixth terms are derived from SOC and the former is an odd function in k space. We define an average energy as follows:

$$AMCA(k) = \frac{MCA(k) + MCA(-k)}{2}, \quad (7)$$

$AMCA(k)$ is the average of $MCA(k)$ and $MCA(-k)$, and the sum of $AMCA(k)$ over k equals to MCA, so the perturbation of the fifth term is eliminated for $AMCA(k)$. Since the sixth term is the perturbation irrelevant to k , the perturbation theory can still be treated as performed by Wang *et al.* [38]. Then the $AMCA$ approximately equals to the sum of the following terms:

$$AMCA(k) = \xi^2 \sum_{\sigma \sigma'} \sum_{o_k, u_k} \frac{M^{\sigma \sigma'}(o_k, u_k)}{E_{u_k}^{\sigma'} - E_{o_k}^{\sigma}}, \quad (8)$$

$$M^{\sigma \sigma'}(o_k, u_k) = \sigma \sigma' \{ |\langle o_k^\sigma | L_z | u_k^{\sigma'} \rangle|^2 - |\langle o_k^\sigma | L_x | u_k^{\sigma'} \rangle|^2 \},$$

where σ (σ') denoting $+$ or $-$ represents the majority or minority spin of occupied (unoccupied) states, and E_o and E_u are the energy levels of the occupied states and the unoccupied states, respectively. As indicated in Eq. (8), the $AMCA$ is large when the energy difference between occupied and unoccupied states is small, or in other words the states near the Fermi energy contribute the largest to $AMCA$. The matrix element $M^{\sigma \sigma'}(o_k, u_k)$ is another important element to calculate $AMCA$. For example, $M^{--}(d_{yz}, d_{z^2})$ is equal to -3 while $M^{--}(d_{x^2-y^2}, d_{xy})$ is equal to 4 for different d orbital states [39,40]. At last, the k -resolved VCMA is defined as follows:

$$VCMA(k) = \frac{\Delta AMCA(k)}{E_{\text{field}}}, \quad (9)$$

where $\Delta AMCA(k)$ is the difference between $AMCA(k)$ with and without electric field, and the E_{field} is the electric field intensity inside insulator (MgO), which is defined positive when the field points to insulator from metal in the Cr/Fe/MgO junction.

All the calculations are performed using density functional theory (DFT) implemented in the Vienna *ab initio* simulation package (VASP) [41,42]. The exchange correlation potential is the Perdew-Burke-Ernzerhof (PBE) generalized gradient approximation (GGA), while the ion-electron interaction is

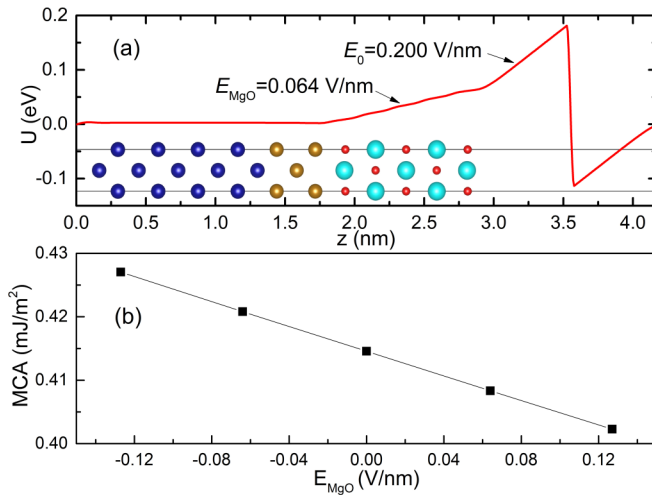


FIG. 1. (a) Calculated electrostatic potential energy across the Cr (9 ML)/Fe (3 ML)/MgO (5 ML)/vacuum (15 Å) supercell and the structure sketch. (b) MCA for Cr/Fe(3 ML)/MgO junction varies with the applied electric field.

described by the projector-augmented plane-wave (PAW) potentials [43–45]. A 500-eV plane-wave cutoff energy and a $51 \times 51 \times 1$ k -point grid are used for MCA calculation, whose uncertainty has been tested and is less than 0.01 meV. The junction structure as shown in Fig. 1(a) is relaxed in the perpendicular direction (z direction) while the in-plane lattice parameter is fixed to 2.866 Å (bulk bcc Fe lattice constant). In our calculation, the large surface magnetization of Cr and the antiferromagnetic coupling at the Cr | Fe interface coincide well with the previous report [46].

III. RESULTS AND DISCUSSIONS

Figure 1(a) shows an example of electrostatic potential energy in the Cr/Fe/MgO/vacuum system with $t_{\text{Fe}} = 3$ MLs. Its slope represents the electric field intensity. The electric field intensity E_{MgO} (E_0) is 0.064 V/nm (0.200 V/nm) in MgO (vacuum). By $\epsilon_{\text{MgO}} = E_0/E_{\text{MgO}}$, the calculated relative dielectric constant of MgO (ϵ_{MgO}) equals 3.1. The experimental $\epsilon_{\text{MgO}}^{\text{expt}}$ is about 9.5 [47]. The plausible reasons for this difference are unrelaxed ions under electric field [27] and the strain effect [48]. We did not relax the ion structure under every applied field because of the unaffordable computational cost. So it should be noted that the effect of ion relaxing on VCMA is not considered in this paper. As an example, Fig. 1(b) shows the linearly field dependent MCA of Cr/Fe/MgO with 3-ML Fe. For all our calculations, the MCA is linearly dependent on the small field E_{MgO} in the range from -0.12 to 0.12 V/nm and the VCMA coefficients were calculated using the slopes.

Figure 2(a) plots the MCA of Cr/Fe/MgO junctions with the Fe layer varying from 1 to 10 MLs. With the increase in t_{Fe} , MCA oscillates strongly at first and then around 1.3 mJ/m² when t_{Fe} is up to 1 nm. Previous investigation of MCA on Fe/MgO shows that the closest (Fe_1) and next closest (Fe_2) Fe MLs adjacent to MgO provide the main contribution to MCA [49], so we plot the layer-resolved MCA contribution from Fe_1 and Fe_2 as shown (the red line) in Fig. 2(a). It is

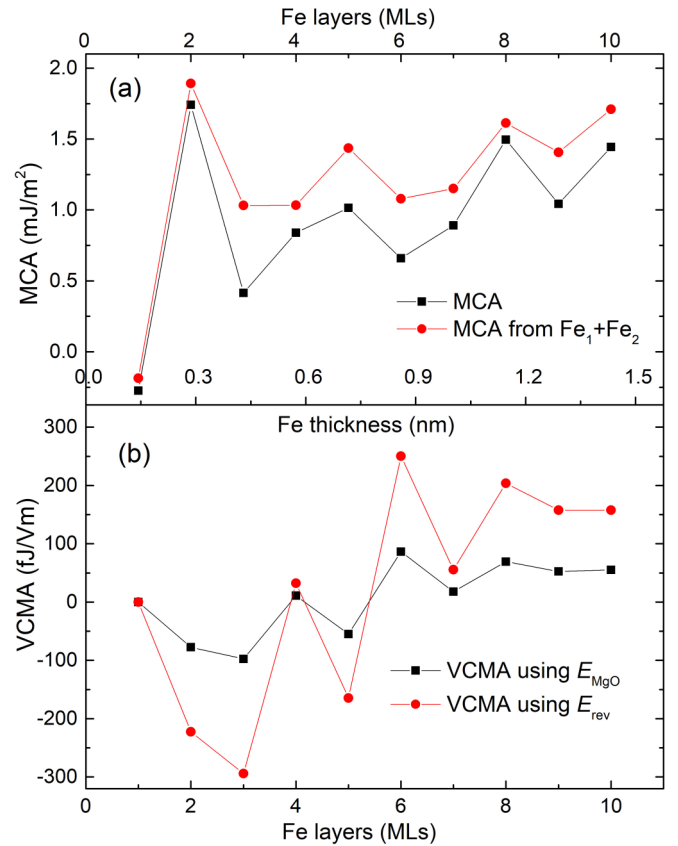


FIG. 2. (a) MCA and (b) VCMA for Cr/Fe/MgO junctions with different number of Fe MLs. For (a), the square and circle represent the total MCA and MCA from $\text{Fe}_1 + \text{Fe}_2$, respectively. For (b), the square and circle represent the VCMA using E_{MgO} and E_{rev} , respectively.

about 1.5 mJ/m² when $t_{\text{Fe}} = 8$ –10 MLs, which is close to the MCA of the Fe/MgO junction [49].

VCMA coefficient calculated using E_{MgO} (black line) as a function of t_{Fe} is shown in Fig. 2(b). The largest VCMA coefficient of -98 fJ/V m is obtained in Cr/Fe/MgO with $t_{\text{Fe}} = 0.43$ nm (one monolayer Fe or half lattice constant of bcc Fe is 1.433 Å). As mentioned in previous investigation [23,27], the electric field-induced atomic displacements in MgO are responsible for ionic contribution to the dielectric constant and produce an additional effect on VCMA. So we take these into account by scaling the electric field in MgO to the $\epsilon_{\text{MgO}}^{\text{expt}}$, namely, $E_{\text{rev}} = E_0/\epsilon_{\text{MgO}}^{\text{expt}}$. The VCMA coefficient calculated using E_{rev} (red line) is also shown in Fig. 2(b), which is about 3 times of the one calculated using E_{MgO} . The corresponding largest VCMA coefficient change to -297 fJ/V m, which matches pretty well with the experimental results of -290 fJ/V m [28]. As shown in Fig. 2(b), the VCMA coefficient oscillates strongly as increasing the t_{Fe} , and changes the sign from negative to positive at a critical t_{Fe} of 5–6-ML Fe. Further the VCMA coefficient decreases quickly with increasing the t_{Fe} from 0.44 to 0.70 nm, also reproducing the observations [28].

The large VCMA for only few Fe MLs and its strong oscillation may naturally be associated with the QW states in the junction, which also sensitively depends on the t_{Fe} .

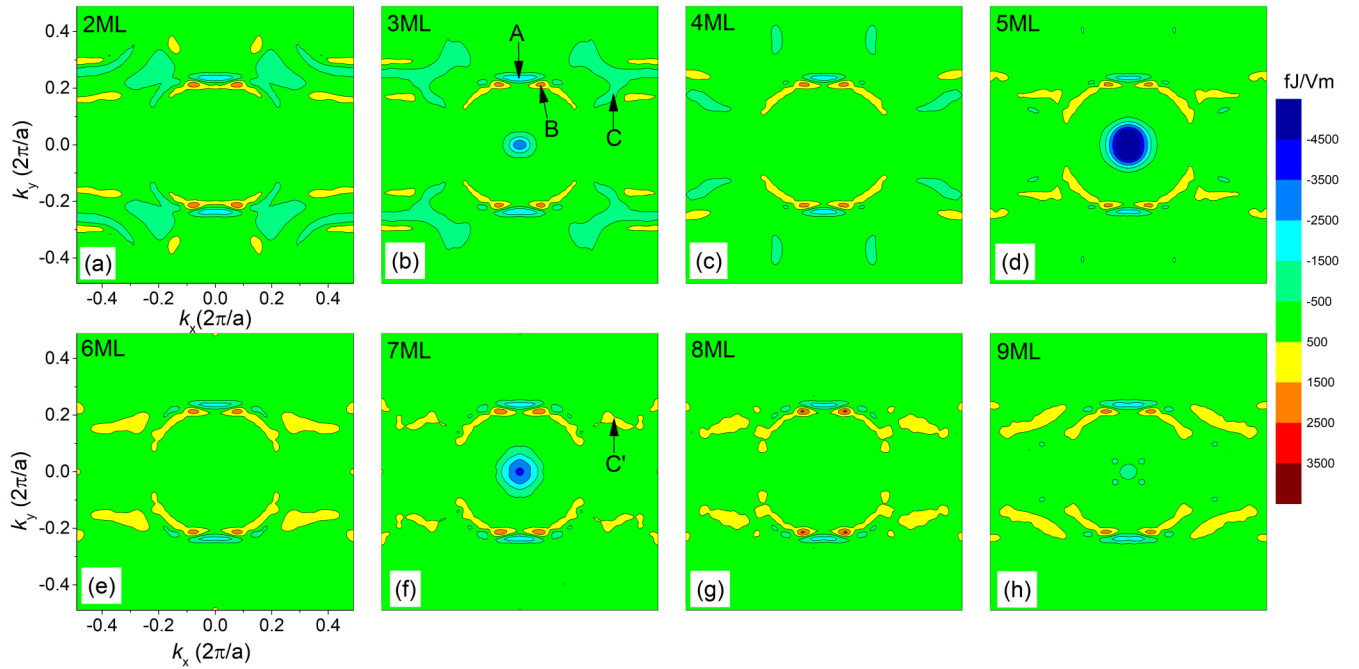


FIG. 3. k -resolved VCMA in the two-dimensional Brillouin zone for Cr/Fe/MgO junctions with different number of Fe MLs from 2 to 9 MLs (a)–(h).

Since the QW states in Cr/Fe/MgO show up at the Γ point in the Brillouin zone, as mentioned in the Introduction, we need to study the VCMA contribution at the Γ point to figure out the relation between the large VCMA and the QW states. Figure 3 plots the k -resolved VCMA in Cr/Fe/MgO with 2–9-ML Fe. Comparing the k -resolved VCMA with different t_{Fe} , there are three important characters worth stressing. First, a large (no) contribution to VCMA at the Γ point for odd-(even-)ML Fe is observed, which results in the oscillating VCMA. This large contribution with negative sign reaches the maximum for $t_{\text{Fe}} = 5$ MLs and becomes very small when t_{Fe} increases to 9 MLs. These properties are likely to associate with QW states. Second, for all of the t_{Fe} , there are two arc-shaped contributions on both sides of the up and down at the k points around $(k_x = 0, k_y = \pm 0.2)$. They have a negative (positive) contribution on the center (left and right) of the arcs. Third, the region of k points around $(k_x = \pm 0.3, k_y = \pm 0.2)$ provides to the VCMA a negative contribution with the t_{Fe} of 2–3 MLs and a positive contribution when the t_{Fe} is larger than 4 MLs, which explains the VCMA sign change.

It has been theoretically reported, with the external electric field, that the screening charge at the metal | insulator interface is responsible for VCMA [4,27]. So we went into the layer-resolved VCMA of the Cr/Fe/MgO junction to check the contributions from the interface and the bulk. Figures 4(a) and 4(b) plot layer-resolved MCA and VCMA for Cr/Fe/MgO junctions with Fe layer varying from 2 to 8 MLs. The labels $\text{Fe}_1, \text{Fe}_2 \dots \text{Fe}_8$ represent the closest, the second closest..., the eighth closest Fe ML to the Fe | MgO interface. As shown in Fig. 4(a), for all the cases, the main MCA contribution locates at Fe_1 , due to the hybridization between the $\text{Fe-}3d_z^2$ and $\text{O-}2p_z$ orbitals as in the previous reference [22]. As for layer-resolved VCMA shown in Fig. 4(b), for the most cases, such as the junctions with 2-, 3-, 6-, 8-ML Fe, the VCMA

contribution has the largest value at Fe_1 and a small value inside the bulk Fe. This is comprehensible because the screening charge locates at the interface, namely Fe_1 . However, for

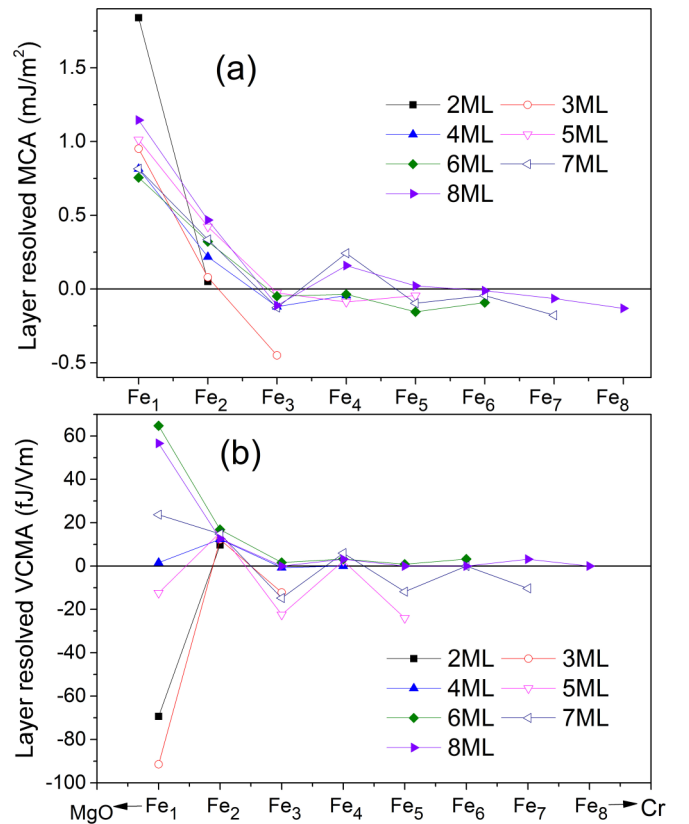


FIG. 4. (a) Layer-resolved MCA and (b) VCMA for Cr/Fe/MgO junctions with Fe layer varying from 2 to 8 MLs.

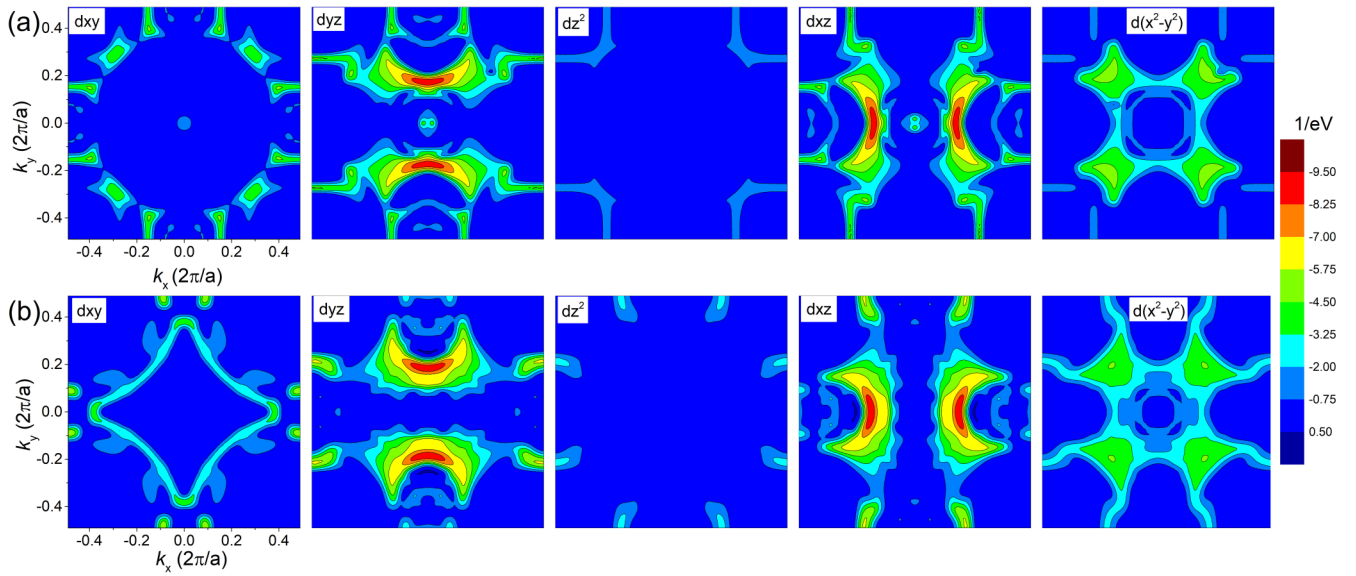


FIG. 5. k -resolved minority partial density of states of interfacial Fe atom (Fe_1) located at Fermi level for Cr/Fe/MgO junctions with (a) 3-ML Fe and (b) 4-ML Fe.

the junction with 5- and 7-ML Fe, the Fe_3 and even Fe_5 still have a large VCMA contribution. What is the origin of this bulk VCMA contribution and is it still relevant to the screening charge at the interface? At the last of this session, we utilized the second perturbation theory based on PDOS to analyze it, and we concluded that the screening charge fills in the delocalized state at the interface resulting in the PDOS redistribution inside the bulk region and then the bulk VCMA contribution.

The screening charge would first fill in the Fermi surface of Fe_1 and then influence the k -resolved VCMA. To further verify the above theory, we compared the Fermi surface located at Fe_1 with the k -resolved VCMA. To display an atom-resolved Fermi surface, we calculated a k -resolved PDOS located at the Fermi level for Fe_1 labeled as $\text{PDOS}(k, E_f, \text{Fe}_1)$. As shown in Fig. 4, for Cr/Fe/MgO junctions with 3- and 4-ML Fe, the d -orbital-resolved PDOSs (k, E_f, Fe_1) with minority states are plotted. Their majority states are not shown here because the majority band at the Fermi level has much smaller DOS than the minority. As we can see, for d_{xy} , d_{yz} , and d_{xz} orbital state, there are (no) spots around the Γ point in Fig. 4(a) [Fig. 4(b)]. This accurately matches that there exists a large (no) VCMA contribution at the Γ point in Cr/Fe/MgO with 3-ML (4-ML) Fe as shown in Figs. 3(b) and 3(c). For both structures with 3- and 4-ML Fe, two arcs on the up and down side in PDOS (k, E_f, Fe_1) of d_{yz} orbital states just correspond to the second character of the k -resolved VCMA. And in the k region of the third character, the Fermi surface of d_{xy} and $d_{x^2-y^2}$ orbital states appear too. Therefore, the charge accumulation on the Fermi surface of Fe_1 to screen the external field is regarded responsible for VCMA.

Now we begin to analyze the three characters of the k -resolved VCMA in detail using the second-order perturbation theory based on the PDOS at a specific k point. And the manner of how the screening charge acts on VCMA will be shown in the following. For the first character, we plot the

PDOS at the Γ point of Fe_1 in the Cr/Fe/MgO junction with 3–6-ML Fe, as shown in Fig. 5. For d_z^2 orbital states, bulk bcc Fe has a half-metal nature, which means there are only majority d_z^2 orbital states across the Fermi level. Since there is a band gap of d_z^2 orbital states for metal Cr and MgO is an insulator, QW states occur for majority d_z^2 orbital states in the Cr/Fe/MgO junction [24]. As we can see, PDOSs of majority d_z^2 orbit (red line) in Fig. 5 split into peaks, and the number of peaks increases while the peak amplitude decreases with increasing the t_{Fe} . Remarkably, one of the quantized d_z^2 orbital peaks locates at the energy very near to the Fermi level for the junctions with 3- and 5-ML Fe. But this peak does not occur for 4- and 6-ML Fe. Besides, taking the case with 3-ML Fe as an example, a peak of minority d_{yz} orbital states locates at the Fermi level, corresponding to the spots at the Γ point of the Fermi surface in Fig. 4(a). According to Eq. (8), these d_{yz} and d_z^2 peaks around the Fermi level would provide a large positive MCA contribution due to the matrix element $M^{+-}(d_{yz}, d_z^2) = +3$. When applying a positive electric field, the positive charge would accumulate at on Fe_1 atoms, and then the d_{yz} peaks would move forward along the energy axis to decrease the occupied PDOS, so the positive MCA energy would decrease resulting in a negative VCMA coefficient. This is how screening charge affects VCMA. In the same way, there is negative (no) VCMA contribution at the Γ point for the junctions with 5-ML (4- and 6-ML) Fe. It can be concluded that the QW states help to provide negative (no) contribution to VCMA for Cr/Fe/MgO junctions with odd (even) MLs Fe resulting in strong VCMA oscillation with respective to t_{Fe} .

Figure 6 plots the orbital-resolved VCMA contribution from Fe_1 . It should be noted that the orbital-resolved VCMA contains all the contribution over the k points in Brillouin zone. Anyway, for the term (d_{yz}, d_z^2), it is a negative (positive) contribution in the case with 3-ML (4-ML) Fe as shown in Fig. 6(a) [Fig. 6(b)]. This just coincides with the negative

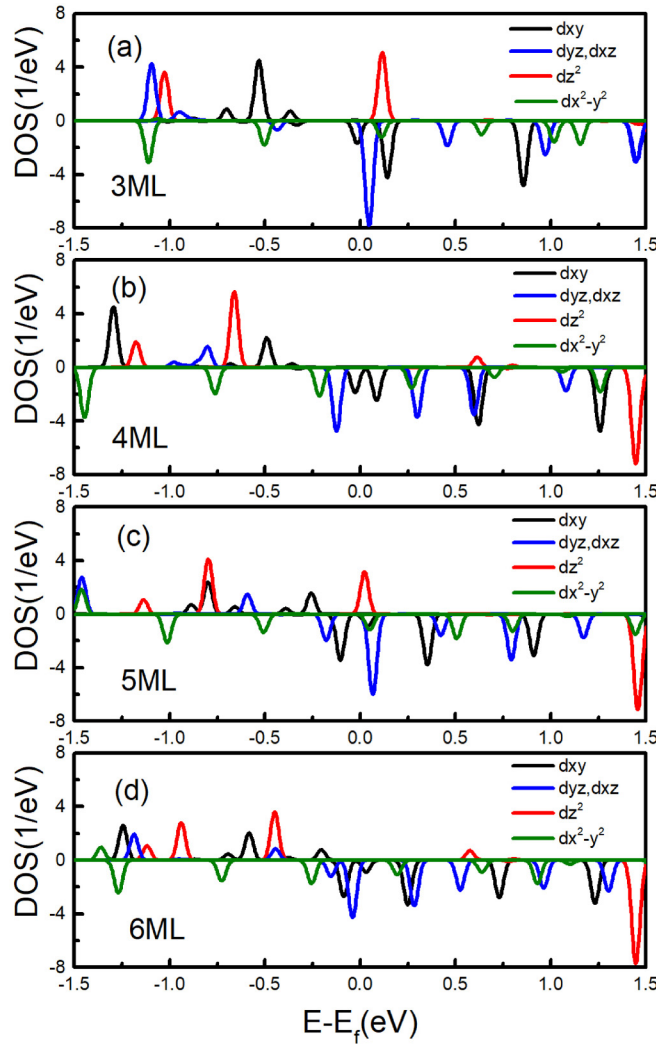


FIG. 6. PDOS at Γ point of two-dimensional Brillouin zone for Cr/Fe/MgO with (a) 3-ML, (b) 4-ML, (c) 5-ML, and (d) 6-ML Fe.

(zero) value of k -resolved VCMA at the Γ point for odd-(even)-ML Fe which is contributed by d_{z^2} QW states and minority d_{yz} orbital peak around the Fermi level. In addition, it can be seen that the terms (d_{xz}, d_{yz}) and $(d_{xy}, d_{x^2-y^2})$ provide a large negative VCMA contribution in the Cr/Fe/MgO junction with 3-ML Fe, too. In a way, these can also be explained using the PDOS at the Γ point as shown in Fig. 5(a). For the terms (d_{xz}, d_{yz}) , the minority d_{xz} and d_{yz} orbital states across the Fermi level are degenerate at the Γ point because of space group C_{4v} owned by the system. And deviating from the Γ point, they split into two energy levels with one occupied and the other unoccupied, which would contribute a large positive MCA energy due to $M^{--}(d_{xz}, d_{yz}) = +1$. When a positive electric field is applied, then the positive charge is accumulated at Fe_1 . The positive MCA would decrease resulting in a negative VCMA contribution. As for the term $(d_{xy}, d_{x^2-y^2})$, a small minority d_{xy} orbital peak and $d_{x^2-y^2}$ peak locate exactly at and above the Fermi level, respectively, which produces a positive MCA with $M^{--}(d_{xy}, d_{x^2-y^2}) = +4$. Analyzing Eq. (8) and the charge accumulation process, this also gives a negative VCMA contribution. In summary,

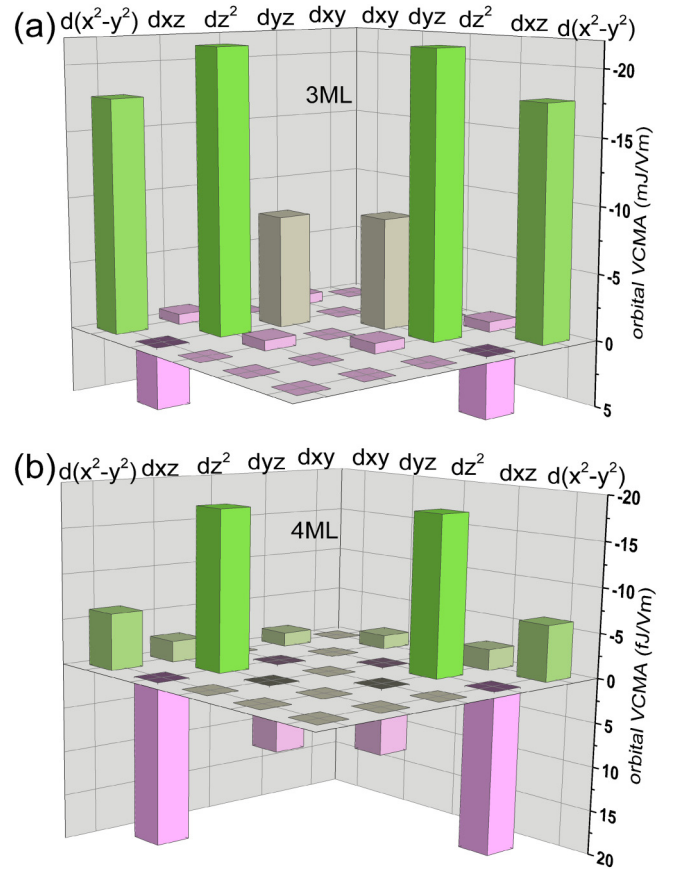


FIG. 7. d -orbital resolved VCMA contribution from Fe_1 for Cr/Fe/MgO with (a) 3-ML and (b) 4-ML Fe.

oscillation of the k -resolved VCMA contribution around the Γ point originates from d_{z^2} QW states and the change of the orbital-resolved Fermi surface at Fe_1 with respect to t_{Fe} .

For the second character, we take the specific k points A and B in the up side arc, as shown in Fig. 3(b), for example, to analyze VCMA using the second-order perturbation theory. Inside the arc, the k -resolved VCMA contribution at k point A (B) is the largest negative (positive) value. Figures 7(a) and 7(b) plot the PDOS of Fe_1 in the Cr/Fe/MgO junction with 3-ML Fe for k points A and B . It can be seen that there is a large minority d_{yz} orbital peak located a little below the Fermi level for both k points A and B , which is confirmed as IRS because of its fast decay inside bulk Fe. When a positive electric field is applied and then positive charge is accumulated, the IRS peaks move toward and cross the Fermi level. Because the more unoccupied states in IRS peaks interact with its occupied states, the absolute value of MCA contribution would be enlarged. We learn from the k -resolved MCA that it is a negative (positive) MCA contribution for k point A (B), so a negative (positive) VCMA contribution is given, just matching the k -resolved VCMA contribution as shown in Fig. 3(b).

At last, for the third character of k -resolved VCMA, we plot the PDOS of Fe_1 for k point C (C') in the junction with 3- (7-)ML Fe as shown in Fig. 3(b) [Fig. 3(f)]. C and C'

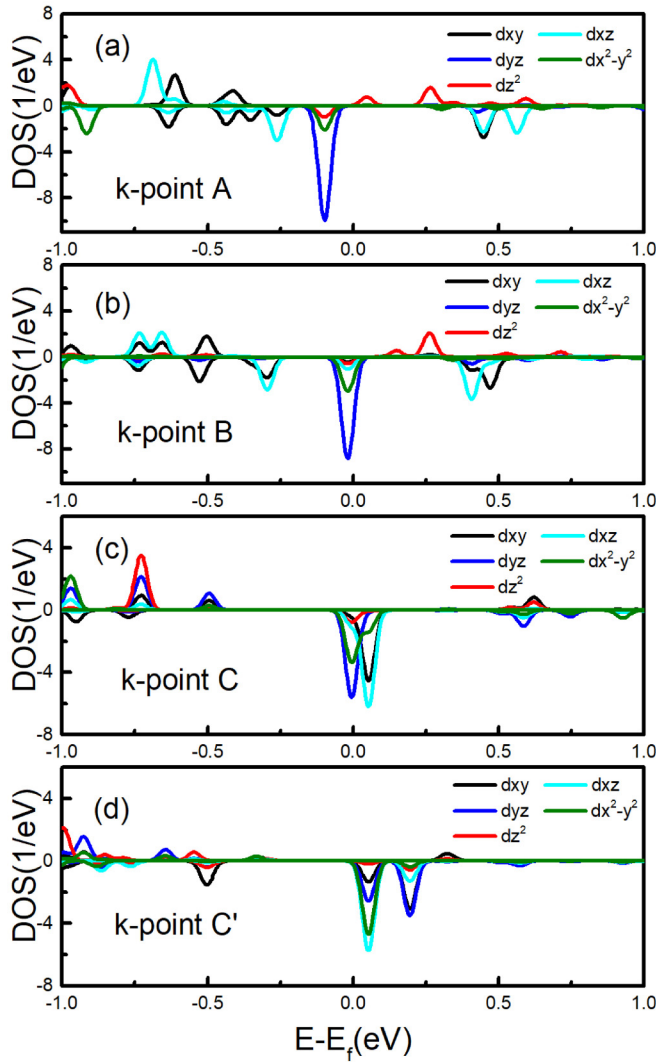


FIG. 8. PDOS at (a) A , (b) B , (c) C k points for Cr/Fe/MgO with 3-ML Fe and (d) C' point with 7-ML Fe. A , B , C , and C' are shown in Figs. 3(b) and 3(f). C' and C are the same k points in Brillouin zone.

are the same k points in the Brillouin zone (see Fig. 8). The remarkable difference from PDOS of C to C' is that one d_{yz} orbital peak moves away from the Fermi level while another d_{xz} orbital peak locates stably a little above the Fermi level, which results in the change of k -resolved VCMA from negative to positive. Therefore, it becomes clear that the change of the Fermi surface with increasing the t_{Fe} of junctions should be responsible for the third character. The origin of the large negative VCMA in Cr/Fe/MgO junctions with ultrathin Fe layer (3 MLs) is a concurrence of the negative contribution in this region and the negative contribution around the Γ point at the same time.

Now we try to explain the bulk VCMA contribution of Fe_3 and Fe_5 in the Cr/Fe/MgO junction with 5-ML Fe using the second perturbation theory based on PDOS. Figure 9(a) [Fig. 9(b)] plots the layer-resolved PDOS around the Fermi level at the Γ point of the Cr/Fe/MgO junction with 3-ML (5-ML) Fe. The PDOSs for two electric fields are shown in Fig. 9, where the solid (dashed) line represents the applied

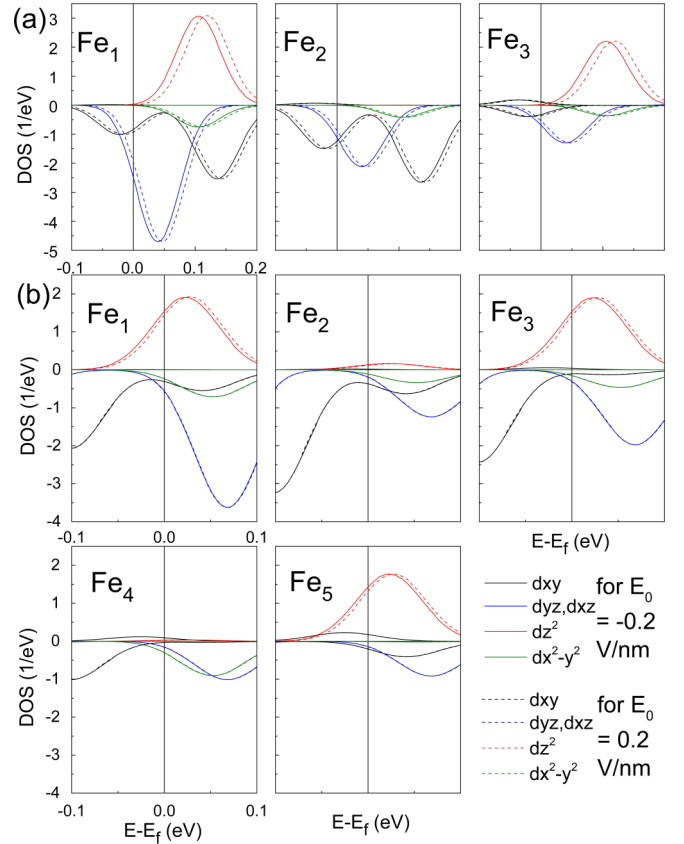


FIG. 9. PDOS near Fermi level at Γ point for every Fe monolayer of the Cr/Fe/MgO junction with (a) 3-ML and (b) 5-ML Fe with applied electric field. The solid (dashed) line represents the applied field in vacuum $E_0 = -0.2$ V/nm ($+0.2$ V/nm).

field in vacuum $E_0 = -0.2$ V/nm ($+0.2$ V/nm). As shown in Fig. 9(a), the PDOS at Fe_1 moves along the positive direction of the energy axis by applying the positive electric field. This means the positive charges accumulate at Fe_1 , which is consistent with the theory of charge screening. According to Eq. (8), the occupied d_{yz} orbital states and unoccupied d_{z^2} orbital states provide the MCA contribution. When the PDOS of d_{yz} orbit moves by applying field, the amount of occupied d_{yz} orbital states decreases and this results in the VCMA contribution. By comparing the PDOS at Fe_1 , Fe_2 , and Fe_3 as shown in Fig. 9(a), we can learn that the amplitude of d_{yz} orbital states is large at Fe_1 and decreases rapidly at Fe_2 and Fe_3 , so that the main VCMA contribution locates at Fe_1 while the contribution of Fe_2 and Fe_3 is small.

In the junction with 5-ML Fe, as shown in Fig. 9(b), the d_{z^2} orbital states intercross the Fermi level. As the quantum well state, it is a delocalized state and spreads over Fe_1 , Fe_3 , and Fe_5 while the amplitude at Fe_2 and Fe_4 is small. Once a positive field applied, the PDOS of the d_{z^2} orbit moves and the occupied d_{z^2} orbital states decreases, resulting in the large (small) VCMA contribution of Fe_1 , Fe_3 , and Fe_5 (Fe_2 and Fe_4). This picture is consistent with the layer-resolved VCMA of the junction with 5-ML Fe shown in Fig. 4(b). Therefore, we conclude that the delocalized state filled by the screening charge results in the PDOS redistribution and VCMA contribution in the bulk region.

IV. CONCLUSION

In summary, we study the origin of large VCMA in Cr/Fe/MgO junctions with ultrathin Fe layer using the first-principles calculation. We find that the VCMA coefficient oscillates strongly with increasing the t_{Fe} and reaches a maximum value of -297 fJ/V m for the system with 3-ML Fe coinciding well with the previous experimental results. Through the k -resolved VCMA and orbital-resolved Fermi surface developed in this paper, we confirmed that the screening charge at the Fe | MgO interface is the direct origin for the VCMA. Combining with the second-order perturbation based on the PDOS for a specific k point, we deduced that the Δ_1 QW states at the Γ point help to provide a large (no) VCMA contribution for junctions with odd- (even-)ML Fe in the range of 2–9. In addition, the change of the orbital-resolved Fermi surface of Fe_1 also plays an important role in the VCMA oscillation. The large VCMA for Cr/Fe/MgO junctions with ultrathin Fe layer are caused by QW states and the change of the orbital-resolved Fermi surface located at Fe_1 together. Finally, it is interesting that IRS can result in some hot spots in the k -resolved VCMA. Our investigation gains insight into

understanding the large VCMA in the Cr/Fe/MgO junction, which could be instructive for designing practical voltage-controlled MRAM devices.

ACKNOWLEDGMENTS

The authors gratefully acknowledge Jia Zhang for his enlightening discussions and help. This project was supported by the National Key Research and Development Program of China (Grants No. 2017YFA0206200, No. 2016YFA0300802, and No. 2018YFB0407600), the National Natural Science Foundation of China (NSFC, Grants No. 51831012, No. 51620105004, No. 51761145110, No. 11674373, and No. 51701203), and partially supported by the Strategic Priority Research Program (B) (Grant No. XDB07030200), the Key Research Program of Frontier Sciences (Grant No. QYZDJ-SSW-SLH016), and the International Partnership Program (Grant No. 112111KYSB20170090) of the Chinese Academy of Sciences (CAS). The work was carried out at the National Supercomputer Center in Tianjin, and the calculations were performed on TianHe-1 (A).

-
- [1] M. Weisheit, S. Fähler, A. Marty, Y. Souche, C. Poinsignon, and D. Givord, *Science* **315**, 349 (2007).
- [2] F. Matsukura, Y. Tokura, and H. Ohno, *Nat. Nanotechnol.* **10**, 209 (2015).
- [3] E. Y. Tsymbal, *Nat. Mater.* **11**, 12 (2012).
- [4] C.-G. Duan, J. P. Velev, R. F. Sabirianov, Z. Zhu, J. Chu, S. S. Jaswal, and E. Y. Tsymbal, *Phys. Rev. Lett.* **101**, 137201 (2008).
- [5] H. Zhang, M. Richter, K. Koepf, I. Opahle, F. Tasnádi, and H. Eschrig, *New J. Phys.* **11**, 043007 (2009).
- [6] K. Nakamura, R. Shimabukuro, Y. Fujiwara, T. Akiyama, T. Ito, and A. J. Freeman, *Phys. Rev. Lett.* **102**, 187201 (2009).
- [7] P. Ruiz-Díaz, T. R. Dasa, and V. S. Stepanyuk, *Phys. Rev. Lett.* **110**, 267203 (2013).
- [8] T. Maruyama, Y. Shiota, T. Nozaki, K. Ohta, N. Toda, M. Mizuguchi, A. A. Tulapurkar, T. Shinjo, M. Shiraishi, S. Mizukami, Y. Ando, and Y. Suzuki, *Nat. Nanotechnol.* **4**, 158 (2009).
- [9] M. Tsujikawa and T. Oda, *Phys. Rev. Lett.* **102**, 247203 (2009).
- [10] W.-G. Wang, M. Li, S. Hageman, and C. L. Chien, *Nat. Mater.* **11**, 64 (2012).
- [11] Y. Shiota, T. Nozaki, F. Bonell, S. Murakami, T. Shinjo, and Y. Suzuki, *Nat. Mater.* **11**, 39 (2012).
- [12] K. Nakamura, T. Akiyama, T. Ito, M. Weinert, and A. J. Freeman, *Phys. Rev. B* **81**, 220409(R) (2010).
- [13] C. Gong, E. M. Kim, Y. Wang, G. Lee, and X. Zhang, *Nat. Commun.* **10**, 2657 (2019).
- [14] U. Bauer, L. Yao, A. J. Tan, P. Agrawal, S. Emori, H. L. Tuller, S. Dijken, and G. S. D. Beach, *Nat. Mater.* **14**, 174 (2015).
- [15] C. Bi, Y. Liu, T. Newhouse-Illige, M. Xu, M. Rosales, J. W. Freeland, O. Mryasov, S. Zhang, S. G. E. te Velthuis, and W. G. Wang, *Phys. Rev. Lett.* **113**, 267202 (2014).
- [16] P. Lukashev, J. D. Burton, S. S. Jaswal, and E. Y. Tsymbal, *J. Phys.: Condens. Matter* **24**, 226003 (2012).
- [17] W. H. Butler, X.-G. Zhang, T. C. Schulthess, and J. M. MacLaren, *Phys. Rev. B* **63**, 054416 (2001).
- [18] J. Mathon and A. Umerski, *Phys. Rev. B* **63**, 220403(R) (2001).
- [19] S. S. P. Parkin, C. Kaiser, A. Panchula, P. M. Rice, B. Hughes, M. Samant, and S. H. Yang, *Nat. Mater.* **3**, 862 (2004).
- [20] S. Yuasa, T. Nagahama, A. Fukushima, Y. Suzuki, and K. Ando, *Nat. Mater.* **3**, 868 (2004).
- [21] S. Ikeda, K. Miura, H. Yamamoto, K. Mizunuma, H. D. Gan, M. Endo, S. Kanai, J. Hayakawa, F. Matsukura, and H. Ohno, *Nat. Mater.* **9**, 721 (2010).
- [22] H. X. Yang, M. Chshiev, B. Dieny, J. H. Lee, A. Manchon, and K. H. Shin, *Phys. Rev. B* **84**, 054401 (2011).
- [23] M. K. Niranjana, C.-G. Duan, S. S. Jaswal, and E. Y. Tsymbal, *Appl. Phys. Lett.* **96**, 222504 (2010).
- [24] S. Miwa, K. Matsuda, K. Tanaka, Y. Kotani, M. Goto, T. Nakamura, and Y. Suzuki, *Appl. Phys. Lett.* **107**, 162402 (2015).
- [25] A. Rajanikanth, T. Hauet, F. Montaigne, S. Mangin, and S. Andrieu, *Appl. Phys. Lett.* **103**, 062402 (2013).
- [26] F. Ibrahim, H. X. Yang, A. Hallal, B. Dieny, and M. Chshiev, *Phys. Rev. B* **93**, 014429 (2016).
- [27] J. Zhang, P. V. Lukashev, S. S. Jaswal, and E. Y. Tsymbal, *Phys. Rev. B* **96**, 014435 (2017).
- [28] T. Nozaki, A. Koziol-Rachwał, W. Skowroński, V. Zayets, Y. Shiota, S. Tamaru, H. Kubota, A. Fukushima, S. Yuasa, and Y. Suzuki, *Phys. Rev. Appl.* **5**, 044006 (2016).
- [29] Q. Xiang, Z. Wen, H. Sukegawa, S. Kasai, T. Seki, T. Kubota, K. Takanashi, and S. Mitani, *J. Phys. D: Appl. Phys.* **50**, 40LT04 (2017).
- [30] A. Koziol-Rachwał, T. Nozaki, K. Freindl, J. Korecki, S. Yuasa, and Y. Suzuki, *Sci. Rep.* **7**, 5993 (2017).
- [31] X. Li, K. Fittell, D. Wu, C. Ty Karaba, A. Buditama, G. Q. Yu, K. L. Wong, N. Altieri, C. Grezes, N. Kioussis, S. Tolbert, Z. Z.

- Zhang, J. P. Chang, P. K. Amiri, and K. L. Wang, *Appl. Phys. Lett.* **110**, 052401 (2017).
- [32] Z. Y. Lu, X. G. Zhang, and S. T. Pantelides, *Phys. Rev. Lett.* **94**, 207210 (2005).
- [33] F. Greullet, C. Tiusan, F. Montaigne, M. Hehn, D. Halley, O. Bengone, M. Bowen, and W. Weber, *Phys. Rev. Lett.* **99**, 187202 (2007).
- [34] T. Niizeki, N. Tezuka, and K. Inomata, *Phys. Rev. Lett.* **100**, 047207 (2008).
- [35] P. Sheng, F. Bonell, S. Miwa, T. Nakamura, Y. Shiota, S. Murakami, D. D. Lam, S. Yoshida, and Y. Suzuki, *Appl. Phys. Lett.* **102**, 032406 (2013).
- [36] D. Bang, T. Nozaki, and Y. Suzuki, *J. Appl. Phys.* **109**, 07C719 (2011).
- [37] X. Wang, D.-S. Wang, R. Wu, and A. J. Freeman, *J. Magn. Mater.* **159**, 337 (1996).
- [38] D.-S. Wang, R. Wu, and A. J. Freeman, *Phys. Rev. B* **47**, 14932 (1993).
- [39] H. Takayama, K.-P. Bohnen, and P. Fulde, *Phys. Rev. B* **14**, 2287 (1976).
- [40] B. S. Yang, J. Zhang, L. N. Jiang, W. Z. Chen, P. Tang, X. G. Zhang, Y. Yan, and X. F. Han, *Phys. Rev. B* **95**, 174424 (2017).
- [41] G. Kresse and J. Furthmüller, *Phys. Rev. B* **54**, 11169 (1996).
- [42] G. Kresse and J. Furthmüller, *Comput. Mater. Sci.* **6**, 15 (1996).
- [43] J. P. Perdew, K. Burke, and M. Ernzerhof, *Phys. Rev. Lett.* **77**, 3865 (1996).
- [44] M. Methfessel and A. T. Paxton, *Phys. Rev. B* **40**, 3616 (1989).
- [45] P. E. Blöchl, *Phys. Rev. B* **50**, 17953 (1994).
- [46] D. F. Johnson, D. E. Jiang, and E. A. Carter, *Surf. Sci.* **601**, 699 (2007).
- [47] M. Wintersgill and Fontanella, *J. Appl. Phys.* **50**, 8259 (1979).
- [48] S. Kwon, P. V. Ong, Q. Sun, F. Mahfouzi, X. Li, K. L. Wang, Y. Kato, H. Yoda, P. K. Amiri, and N. Kioussis, *Phys. Rev. B* **99**, 064434 (2019).
- [49] A. Hallal, H. X. Yang, B. Dieny, and M. Chshiev, *Phys. Rev. B* **88**, 184423 (2013).